Analysis of Transmit Diversity Performance over Vertical FSO Channels with Altitude-Dependent Impairments

Neha Tiwari, Swades De, and Dharmaraja Selvamuthu

***Abstract*—This paper studies the performance of transmit diversity schemes over high altitude platform-to-ground vertical free-space optical (VFSO) link under various channel impairments. Unlike conventional independent layered channel model, it considers concatenated vertical channel, modeled using N^* gamma-gamma distributions. Wavelength and time diversity techniques are considered and the effectiveness in mitigating atmospheric turbulence and pointing errors is studied in terms of average bit error rate (ABER). The derived closed-form ABER expressions are shown to match well with Monte-Carlo simulation of VFSO channel using correlated phase screen method. Numerical results show that under strong turbulence time diversity offers 7.5 dB gain over wavelength diversity in achieving an ABER of 10^{-4}, whereas wavelength diversity outperforms time diversity by 10 dB where pointing error dominates.**

***Index Terms*—Transmit diversity, HAP-to-ground vertical FSO link, concatenated channel model, pointing error, BER analysis**

I. Introduction

Free space optical (FSO) communication from high-altitude platforms (HAPs) to ground nodes offers high data rates and enhanced spectral efficiency for aerial backhaul. However, vertical FSO (VFSO) links face impairments due to altitude-dependent turbulence and dynamic pointing errors due to HAP mobility and wind-induced jitter. Diversity methods are commonly used to mitigate the performance degradation. Prior studies primarily focused on receiver-end diversity. For example, [1] studied multiple-input single-output FSO channels with detector arrays, and [2] derived average bit error rate (ABER) expressions for vertical underwater optical links. In contrast, transmit diversity is more effective for VFSO links, as it mitigates impairments with low receiver complexity.

Most existing studies on transmit diversity [3]–[5] assume homogeneous turbulence, which limits their applicability to vertical links. A layered model was proposed in [6] where each segment is represented by a Gamma-Gamma (GG) distribution. While Málaga, Double-GG, and Fisher-Snedecor models are effective for homogeneous or horizontally uniform fading, N^*GG model enables a segment-wise representation of turbulence, where each layer is characterized by altitude-dependent refractive index ($C_n^2(h)$) variation. Its multiplicative form also facilitates tractable derivation of communication performance, balancing physical realism with analytical tractability.

This work was supported in part by THDC under grant THDC/RKSH/R&D/F-2076/1036, in part by the SERB, India, under grant CRG/2023/005421, in part by DST-RSF research project no. 22-49-02023 (RSF), and in part by research project no. 64800 (DST).

Neha Tiwari is with Bharti School of Telecommunication, IIT Delhi, New Delhi, India (Email: bsz208010@dbst.iitd.ac.in). Swades De is with the Department of Electrical Engineering, IIT Delhi, New Delhi, India (Email: swadesd@ee.iitd.ac.in). Dharmaraja Selvamuthu is with Department of Mathematics, IIT Delhi, New Delhi, India (Email: dharmar@maths.iitd.ac.in).

Unlike prior studies that treat turbulence and misalignment in isolation or under homogeneous channel assumptions [3]–[5], this work explicitly models the VFSO link across multiple turbulence regimes using an altitude-dependent N^*GG layered fading model. In addition, we introduce a dynamic pointing error model that incorporates time varying angular jitter due to wind-induced drift, platform vibrations, and angle of arrival, thereby capturing realistic HAP motion. *To the best of our knowledge, this is the first analytical study to jointly evaluate transmit diversity over layered VFSO channels.*

Our key contributions are as follows: (1) The performance of transmit diversity schemes in VFSO channel are studied under jointly modeled altitude-dependent turbulence, absorption loss, and pointing errors. (2) Closed-form expressions for ABER are derived for the competitive schemes, which are validated via Monte-Carlo simulations using the correlated phase screen method. (3) An asymptotic analysis is presented to find diversity orders and quantify coding gain. (4) Robustness study is conducted to assess sensitivity to turbulence strength, pointing error, and the number of channel layers. (5) A key design insight is reported: time diversity outperforms wavelength diversity under strong turbulence, while wavelength diversity is more effective under severe misalignment.

II. System Model

We consider a VFSO system between HAP and ground terminal, consisting of $k = 1, \cdots, K$ photodetectors (PDs). The HAP transmits over distinct channel resource (wavelength or time slot), and each ground PD is tuned to a specific channel resource. PD_k detects the k^{th} component. The received signal at PD_k is $y_k = h_{k,N}\gamma_k x + \nu$, where $h_{k,N} = h_{l,k,N} \cdot h_{t,k,N} \cdot h_{p,k,N}$ is the layered channel coefficient over N vertical layers, γ_k is the responsivity of the PD_k, x is the transmitted symbol, and ν is zero-mean Gaussian noise. $h_{l,k,N}$ accounts for absorption losses, $h_{t,k,N}$ captures turbulence-induced fading, and $h_{p,k,N}$ models geometric spread and misalignment loss. The instantaneous signal-to-noise ratio (SNR) is

$$\text{SNR}(h_{k,N}) = \frac{\gamma_k^2 h_{k,N} P_k}{K\sigma_c^2} \tag{1}$$

where P_k is the transmitted power and σ_c^2 is the noise variance.

A. Atmospheric Attenuation and Vertical Optical Turbulence

Over a VFSO link of height H, the attenuation follows Beers-Lambert law: $h_{l,k,n} = \exp(-H\wp)$ [7], where $\wp$ is the attenuation coefficient in dB/km. The irradiance fading varies with height; turbulence eddies near ground tend to be spherical and symmetrical [8], but they become increasingly anisotropic and asymmetrical at higher altitudes. Recognizing these altitude-

based variations, the work in [6] proposed segmenting the VFSO channel into parallel layers and developed a channel model that relies on a cascaded structure of fading coefficients for each layer $h_{t,k,n}$. The overall vertical optical turbulence fading coefficient is modeled as $h_{t,k,N} = \prod_{n=1}^{N} h_{t,k,n}$ where $h_{t,k,n}$ for each layer is independent and non-identically distributed and follows GG distribution with different scintillation parameters $\alpha_{k,n}$ and $\beta_{k,n}$. The PDF of overall fading coefficient $h_{t,k,N}$ follows a N^*GG distribution and is given as

$$f_{h_{t,k,N}}(x) = \Upsilon G_{0,2N}^{2N,0}\left(\left(\prod_{n=1}^{N}(\alpha_{k,n}\beta_{k,n})\right)x\middle|\begin{matrix}\cdots\\ \Xi\end{matrix}\right) \quad (2)$$

where $\Upsilon = \frac{\prod_{n=1}^{N}(\alpha_{k,n}\beta_{k,n})}{\prod_{n=1}^{N}(\Gamma(\alpha_{k,n})\Gamma(\beta_{k,n}))}$ and $\Xi = \alpha_{k,1} - 1, \cdots, \alpha_{k,N} - 1, \beta_{k,1} - 1, \cdots, \beta_{k,N} - 1$.

Remark 1. *The considered N^*GG model balances physical fidelity for altitude-dependent layered turbulence and analytical tractability. Replacing GG with more general fading families, e.g., Málaga, Fisher-Snedecor, requires layer-wise calibration data that are currently unavailable for HAP altitudes.*

B. Boresight and Angular Jitter-Induced Misalignment Fading

In VFSO systems, beam misalignment occurs due to a combination of static displacements and dynamic orientation jitter due to platform vibrations, thermal drift, wind disturbances, turbulence-induced beam wander, and angle-of-arrival (AoA) fluctuations [9], [10]. To capture these effects comprehensively, we model total radial displacement r at receiver as

$$r = \sqrt{(x + H\theta_x)^2 + (y + H\theta_y)^2} \quad (3)$$

where (x, y) are static lateral displacements due to platform misalignment, (θ_x, θ_y) represents angular jitter from beam wander, tracking drift, or AoA-induced deviations [11], [12].

$$x \sim \mathcal{N}(\phi_x, \rho_x^2), \quad y \sim \mathcal{N}(\phi_y, \rho_y^2), \quad \theta_x, \theta_y \sim \mathcal{N}(0, \sigma_0^2). \quad (4)$$

ϕ_x, ϕ_y denote non-zero boresight offsets; σ_0^2 is the variance of angular fluctuations. To capture the impact of temporal variation in HAP orientation, we include temporal angular jitter as well. Per-slot angular jitter is modeled as $\sigma_0^2(t) = \sigma_{\text{base}}^2 + \Delta_{\text{dyn}}(t)$, where σ_{base}^2 is the nominal jitter variance, and $\Delta_{\text{dyn}}(t)$ is the additional jitter introduced by external perturbations in time slot t. We assume $\Delta_{\text{dyn}}(t)$ is sampled independently per time slot from a zero-mean Gaussian process. The effective displacement variances are modeled as a function of t:

$$\rho_{x,\text{eff}}^2(t) = \rho_x^2 + H^2\sigma_0^2(t), \quad \rho_{y,\text{eff}}^2(t) = \rho_y^2 + H^2\sigma_0^2(t). \quad (5)$$

The radial displacement r is approximately Rician distributed. The corresponding misalignment fading coefficient is

$$h_{p,k,N}(r; H) \approx A_0 \exp\left(-\frac{2r^2}{w_{H_{\text{eq}}}^2}\right), \quad r \geq 0 \quad (6)$$

where $w_{H_{\text{eq}}}$ is the equivalent beam waist at distance H, $A_0 = [\text{erf}(\nu)]^2$ is the maximum fraction of collected power under perfect alignment conditions, $\nu = \frac{\sqrt{\pi} r_a}{\sqrt{2} w_\zeta}$, $w_\zeta = \theta_H H$. The probability density function of $h_{p,k,N}$ is given by

$$f_{h_{p,k,N}}(h) = \frac{z_p^2}{A_{p,k,N}^{z_p^2}} h^{z_p^2 - 1}, \quad 0 \leq h \leq A_{p,k,N} \quad (7)$$

where the shaping parameter is defined as $z_p^2(t) = \frac{w_{H_{\text{eq}}}^2}{4}\left(\frac{M(t)}{2}\right)^{-1/3}$, with $M(t) = 3\phi_x^2\rho_{x,\text{eff}}^4(t) + 3\phi_y^2\rho_{y,\text{eff}}^4(t) + \phi_x^6 + \phi_y^6$, and the peak misalignment fading coefficient is

$$A_{p,k,N}(t) = A_0 \exp\left(\frac{1}{z_p^2(t)} - \frac{1}{2\psi_x^2} - \frac{1}{2\psi_y^2} - \frac{\phi_x^2}{2\rho_{x,\text{eff}}^2(t)\psi_x^2} - \frac{\phi_y^2}{2\rho_{y,\text{eff}}^2(t)\psi_y^2}\right) \quad (8)$$

with $\psi_x = \frac{w_{H_{\text{eq}}}}{2\rho_{x,\text{eff}}(t)}$ and $\psi_y = \frac{w_{H_{\text{eq}}}}{2\rho_{y,\text{eff}}(t)}$ and all terms in $\exp(\cdot)$ are normalized with respect to $w_{H_{\text{eq}}}$ for dimensional consistency.

Remark 2. *Unlike prior works that assume static misalignment, we introduce a time-slot-indexed model for angular jitter, capturing temporal misalignment dynamics due to HAP drift, vibration, and atmospheric effects.*

C. Composite Concatenated Channel Model

The PDF of N^*GG VFSO fading channel gain is found using

$$f_{h_{k,N}}(h) = \int f_{h|h_{t,k,N}}(h|h_{t,k,N}) f_{h_{t,k,N}}(h_{t,k,N}) dh_{t,k,N}. \quad (9)$$

$f_{h|h_{t,k,N}}(h|h_{t,k,N}) = \frac{1}{h_{l,k,N}h_{t,k,N}} f_{h_{p,k,N}}(h|(h_{l,k,N}h_{t,k,N}))$ is the probability conditioned on $h_{p,k,N}$. Substituting (2) and (7) in (9), $f_{h_{k,N}}(h)$ is given by (11).

III. Transmitter Diversity Analysis using Polarization Shift Keying (PolSK) Scheme

One mitigation technique for VFSO link degradation to impairments is transmit diversity. In this section ABER derivation is done for a PolSK-based concatenated VFSO system model for no diversity, wavelength diversity and time diversity cases.

A. No Diversity

For an FSO system with single transmitter and receiver and using PolSK, the conditional BER is given by $P_{ec}(h) = \frac{1}{2}\text{erfc}\left(\sqrt{\frac{\gamma^2 hP}{2\sigma_c^2}}\right)$ [13], where γ is responsivity, σ_c^2 is the channel noise variance and P is the local oscillator power. The ABER is obtained as: $P_e = \int_0^\infty P_{ec}(h) f_{h_{k,N}}(h) dh$.

Theorem 1. *The expression for ABER of a PolSK-based N^*GG FSO link with pointing error and single transmit and receive antenna is given by* (12).

Proof. By substituting the expression for $f_{k,N}(h)$ using (11) and $P_{ec}(h)$ in the expression of P_e, we obtain (13). Expressing complementary error function erfc$(\cdot)$ as Meijer G-function we get (13) as (14). Using ([14], 07.34.21.0011.01) for further simplifications we lead to the final form of (12). □

B. Wavelength Diversity

The conditional BER of VFSO link with wavelength diversity over multiple atmospheric channels, $k = 1, 2, \cdots, K$ is given by $P_{ec}(h_{k,N}) = Q(\sqrt{SNR})$ [13]. By substituting (1) in the expression of $P_{ec}(h_{k,n})$, we get the conditional BER as

$$P_{ec}(h_{k,N}) = Q\left(\frac{\gamma_k\sqrt{P_k}}{\sqrt{K}\sigma_c}\sqrt{\sum_{k=1}^{K} h_{k,N}}\right), \quad (10)$$

γ_k is the responsivity of PD$_k$, $Q(\cdot)$ is the Q function. The ABER is obtained as: $P_e = \int_0^\infty P_{ec}(h_{k,N}) f_{h_{k,N}}(h_{k,N}) dh_{k,N}$.

Theorem 2. *ABER of a PolSK-based N^*GG FSO link with pointing error and wavelength diversity is given by* (15).

Proof. Substituting (11) and (10) in the expression of P_e, we obtain (16). Using the approximation of Q-function [15] and substituting in (16) we get the wavelength diversity ABER in (17). Using Meijer G-function for expressing the $\exp(-x)$ as $G_{0,1}^{1,0}\left[x\middle|\begin{matrix}-\\0\end{matrix}\right]$, the ABER of PolSK-based FSO system is obtained in (18) using ([14], 07.34.21.0011.01). Writing (18) in terms of average SNR, the ABER is obtained as (15). □

C. Time Diversity

In this case a single transmitter and receiver is used. Therefore $\lambda_{1,N} = \lambda_{2,N} = \cdots = \lambda_{k,N} = \lambda_N$, where $\alpha_{1,N} = \alpha_{2,N} = \cdots = \alpha_{k,N} = \alpha_N$ and $\beta_{1,N} = \beta_{2,N} = \cdots = \beta_{k,N} = \beta_N$ [16]. Substituting these in (15), the expression of ABER for time diversity of a PolSK-based N^*GG FSO link with pointing error is obtained and is given by (19).

$$f_{h_{k,N}}(h) = \Upsilon \frac{z_p^2}{A_{p,k,N} h_{l,k,N}} G_{1,2N+1}^{2N+1,0}\left(\frac{\mathcal{A}_k\, h}{A_{p,k,N} h_{l,k,N}}\middle| \begin{matrix} z_p^2 \\ z_p^2 - 1, \Xi \end{matrix}\right). \quad (11)$$

$$P_e^{(nd)} = \frac{z_p^2}{2\sqrt{\pi}\,\mathcal{G}_k}\, G_{2N+2,3}^{2,2N+1}\left(\frac{\gamma^2 P\, A_{p,k,N} h_{l,k,N}}{2\sigma_c^2\, \mathcal{A}_k}\middle| \begin{matrix} 1, 1 - z_p^2, -\Xi \\ 0, 0.5, -z_p^2 \end{matrix}\right) \quad (12)$$

$$\begin{aligned} P_e = \Upsilon \frac{z_p^2}{A_{p,k,N} h_{l,k,N}} \int_0^\infty \frac{1}{2} \operatorname{erfc}\left(\sqrt{\frac{\gamma^2 h P}{2\sigma_c^2}}\right) \\ \times G_{1,2N+1}^{2N+1,0}\left(\frac{\mathcal{A}_k\, h}{A_{p,k,N} h_{l,k,N}}\middle| \begin{matrix} z_p^2 \\ z_p^2 - 1, \Xi \end{matrix}\right) dh \end{aligned} \quad (13)$$

$$\begin{aligned} P_e = \Upsilon \frac{z_p^2}{2\sqrt{\pi} A_{p,k,N} h_{l,k,N}} \int_0^\infty G_{1,2}^{2,0}\left(\frac{\gamma^2 h P}{2\sigma_c^2}\middle| \begin{matrix} 1 \\ 0, 1/2 \end{matrix}\right) \\ \times G_{1,2N+1}^{2N+1,0}\left(\frac{\mathcal{A}_k\, h}{A_{p,k,N} h_{l,k,N}}\middle| \begin{matrix} z_p^2 \\ z_p^2 - 1, \Xi \end{matrix}\right) dh \end{aligned} \quad (14)$$

$$\begin{aligned} P_e^{(wd)} \approx \frac{1}{12} \prod_{k=1}^{K} \frac{z_p^2}{\mathcal{G}_k}\, G_{2N+1,2}^{1,2N+1}\left[\frac{A_{p,k,N}\, \overline{\mathrm{SNR}}}{2K\, \mathcal{A}_k}\middle| \begin{matrix} 1 - z_p^2, & -\Xi \\ 0, & -z_p^2 \end{matrix}\right] \\ + \frac{1}{4} \prod_{k=1}^{K} \frac{z_p^2}{\mathcal{G}_k}\, G_{2N+1,2}^{1,2N+1}\left[\frac{2A_{p,k,N}\, \overline{\mathrm{SNR}}}{3K\, \mathcal{A}_k}\middle| \begin{matrix} 1 - z_p^2, & -\Xi \\ 0, & -z_p^2 \end{matrix}\right] \end{aligned} \quad (15)$$

$$\begin{aligned} P_e = \prod_{k=1}^{K} \Upsilon \frac{z_p^2}{A_{p,k,N} h_{l,k,N}} \int_0^\infty Q\left(\frac{\gamma_k \sqrt{P_k}}{\sqrt{K}\sigma_c} \sqrt{\sum_{k=1}^{K} h_{k,N}}\right) \\ \times G_{1,2N+1}^{2N+1,0}\left(\frac{\mathcal{A}_k\, h_{k,N}}{A_{p,k,N} h_{l,k,N}}\middle| \begin{matrix} z_p^2 \\ z_p^2 - 1, \Xi \end{matrix}\right) dh_{k,N} \end{aligned} \quad (16)$$

$$\begin{aligned} P_e \approx \prod_{k=1}^{K} \frac{\Upsilon z_p^2}{A_{p,k,N} h_{l,k,N}} \int_0^\infty G_{1,2N+1}^{2N+1,0}\left(\frac{\mathcal{A}_k h_{k,N}}{A_{p,k,N} h_{l,k,N}}\middle| \begin{matrix} z_p^2 \\ z_p^2 - 1, \Xi \end{matrix}\right) \\ \times \left[\frac{1}{12} e^{-\frac{\gamma_k^2 h_{k,N} P_k}{2K\sigma_c^2}} + \frac{1}{4} e^{-\frac{2\gamma_k^2 h_{k,N} P_k}{3K\sigma_c^2}}\right] dh_{k,N} \end{aligned} \quad (17)$$

$$\begin{aligned} P_e \approx \frac{1}{12} \prod_{k=1}^{K} \frac{z_p^2}{\mathcal{G}_k}\, G_{2N+1,2}^{1,2N+1}\left[\frac{\gamma_k^2 P_k A_{p,k,N} h_{l,k,N}}{2K\sigma_c^2\, \mathcal{A}_k}\middle| \begin{matrix} 1 - z_p^2, -\Xi \\ 0, -z_p^2 \end{matrix}\right] \\ + \frac{1}{4} \prod_{k=1}^{K} \frac{z_p^2}{\mathcal{G}_k}\, G_{2N+1,2}^{1,2N+1}\left[\frac{2\gamma_k^2 P_k A_{p,k,N} h_{l,k,N}}{3K\sigma_c^2\, \mathcal{A}_k}\middle| \begin{matrix} 1 - z_p^2, -\Xi \\ 0, -z_p^2 \end{matrix}\right] \end{aligned} \quad (18)$$

$$\begin{aligned} P_e^{(td)} \approx \frac{1}{12} \left[\frac{z_p^2}{\mathcal{G}_N}\right]^K \left[G_{2N+1,2}^{1,2N+1}\left(\frac{A_{p,N}\, \overline{\mathrm{SNR}}}{2K\, \mathcal{A}_N}\middle| \begin{matrix} 1 - z_p^2, -\Xi \\ 0, -z_p^2 \end{matrix}\right)\right]^K \\ + \frac{1}{4} \left[\frac{z_p^2}{\mathcal{G}_N}\right]^K \left[G_{2N+1,2}^{1,2N+1}\left(\frac{2A_{p,N}\, \overline{\mathrm{SNR}}}{3K\, \mathcal{A}_N}\middle| \begin{matrix} 1 - z_p^2, -\Xi \\ 0, -z_p^2 \end{matrix}\right)\right]^K \end{aligned} \quad (19)$$

$$C_0^{(wd)} = \prod_{k=1}^{K} \left[\frac{z_{p,k}}{2\sqrt{\pi}\,\mathcal{G}_k} \left(\frac{\gamma^2 P A_{p,k} h_{l,k}}{2\sigma_c^2\, \mathcal{A}_k}\right)^{-z_{p,k} \min_n(\alpha_{k,n}, \beta_{k,n})}\right] \quad (20)$$

$$C_0^{(td)} = \prod_{k=1}^{K} \left[\frac{z_p}{2\sqrt{\pi}\,\mathcal{G}_k} \left(\frac{\gamma^2 P A_p h_l}{2\sigma_c^2\, \mathcal{A}_k}\right)^{-z_p \min_n(\alpha_{k,n}, \beta_{k,n})}\right] \quad (21)$$

Here, $\mathcal{A}_k = \prod_{n=1}^{N} (\alpha_{k,n}\beta_{k,n})$, $\mathcal{G}_k = \prod_{n=1}^{N} \Gamma(\alpha_{k,n})\Gamma(\beta_{k,n})$.

D. Asymptotic ABER and Diversity Gain

To study the high-SNR behavior of the considered links, we derive the asymptotic ABER and diversity order expressions. The *asymptotic diversity order* (ADO) is defined as [11]

$$\mathrm{ADO} = \lim_{\overline{\mathrm{SNR}} \to \infty} \left(-\frac{\partial \ln P_e}{\partial \ln \overline{\mathrm{SNR}}}\right). \quad (22)$$

Here, $\overline{\mathrm{SNR}}$ denotes average SNR and P_e is the ABER.

In no-diversity case, the received signal undergoes N^*GG fading and pointing error. Using asymptotic expansion of the Meijer-G function, the approximated ABER at high SNR is

$$P_e^{(nd)} \sim C_0^{(nd)} \cdot (\overline{\mathrm{SNR}})^{-z_p \cdot \min_n(\alpha_n, \beta_n)} \quad (23)$$

with the coding gain

$$C_0^{(nd)} = \frac{z_p}{2\sqrt{\pi}\,\mathcal{G}} \left(\frac{\gamma^2 P A_p h_l}{2\sigma_c^2 \mathcal{A}}\right)^{-z_p \cdot \min_n(\alpha_n, \beta_n)} \quad (24)$$

where $\mathcal{A} = \prod_{n=1}^{N} (\alpha_n \beta_n)$ and $\mathcal{G} = \prod_{n=1}^{N} \Gamma(\alpha_n)\Gamma(\beta_n)$.

In K-branch wavelength diversity, the asymptotic ABER is

$$P_e^{(wd)} \sim C_0^{(wd)} \cdot (\overline{\mathrm{SNR}})^{-\sum_{k=1}^{K} z_{p,k} \cdot \min_n(\alpha_{k,n}, \beta_{k,n})} \quad (25)$$

where the coding gain $C_0^{(wd)}$ is given in (20).

For time diversity with K independent time slots, we have

$$P_e^{(td)} \sim C_0^{(td)} \cdot (\overline{\mathrm{SNR}})^{-z_p \cdot \sum_{k=1}^{K} \min_n(\alpha_{k,n}, \beta_{k,n})} \quad (26)$$

with $C_0^{(td)}$ given in (21). Table I summarizes the ADO expressions. These results show that wavelength diversity aggregates diversity gains across independently misaligned spectral branches, whereas time diversity gains from temporal fading decorrelation under a common pointing error profile.

Remark 3. *The derived ADO expressions highlight the need for jointly considering layered turbulence and pointing error across the diversity branches for designing robust VFSO links.*

Claim 1. *In HAP-to-ground VFSO link, the optimal transmit diversity depends on the dominant channel impairment.*

Proof. **Time diversity under dominant turbulence:** Here, the same signal is sent over K slots. If the channel coherence time is smaller than the slot size, the fading across the slots is independent. Denoting the outage probability for one slot by $P_{\mathrm{out},s}$, the overall outage is $P_{\mathrm{out}}^{(td)} = P_{\mathrm{out}_s}^{K}$. Since N^*GG fading has long-tailed distribution in strong turbulence (Fig. 1), individual slot outages are high, but time diversity suppresses

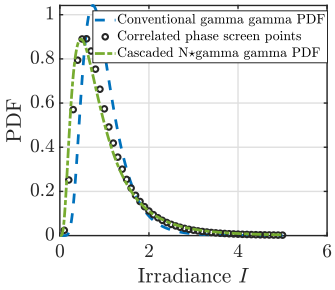

Fig. 1: N^*GG PDF for HAP-ground VFSO link [6].

TABLE I: ADO under layered turbulence and pointing errors

Scheme	Diversity order expression
No diversity	$z_p \cdot \min_n(\alpha_n, \beta_n)$
Wavelength diversity	$\sum_{k=1}^{K} z_{p,k} \cdot \min_n(\alpha_{k,n}, \beta_{k,n})$
Time diversity	$z_p \cdot \sum_{k=1}^{K} \min_n(\alpha_{k,n}, \beta_{k,n})$

this via exponential decay, i.e., the gain scales as $\mathcal{O}(K)$.

Wavelength diversity under dominant pointing error: Here, transmission uses K wavelengths. In strong turbulence, nearby wavelengths face correlated fading, as $\rho_{\lambda_1,\lambda_2} = e^{-c(\Delta\lambda)^2}$, where c is an atmospheric constant. As closer wavelengths are highly correlated, the diversity gain is weaker in turbulence fading. In contrast, with high pointing errors, wavelength diversity is more effective because different wavelengths experience different pointing errors, thus increasing the chances of receiver alignment with at least one wavelength. □

IV. Numerical Results

The derived expressions are validated using 5×10^6 correlated phase screen (CPS)-based Monte-Carlo simulations. Unless otherwise stated, $\lambda = 1550\,\text{nm}$, $\gamma_k = 0.9$, optical bandwidth $= 10\,\text{nm}$, electrical bandwidth $= 1\,\text{GHz}$, zenith angle $\zeta = 40°$, link altitude $H = 25\,\text{km}$, RMS wind speed $V_\omega = 21\,\text{m/s}$, and $C_n^2(0) = 1.7 \times 10^{-13}\,\text{m}^{-2/3}$. Layer-wise (α, β) are obtained from altitude-dependent $C_n^2(h)$ (HV model) via Rytov variance σ_I^2 and GG moment matching, ensuring $\mathbb{E}\{h\} = 1$. Receiver aperture radius $r_a = 5\text{-}10\,\text{cm}$ and beam spot to aperture ratio $w_Z/r_a \gg 1$; dynamic misalignment is modeled with (i) small-angle orientation jitter $\sigma_0 = 0.1\text{-}1\,\text{mrad}$ and (ii) position vibration $\sigma_d \approx 0.4\,\text{m}$ at the focal plane [1].

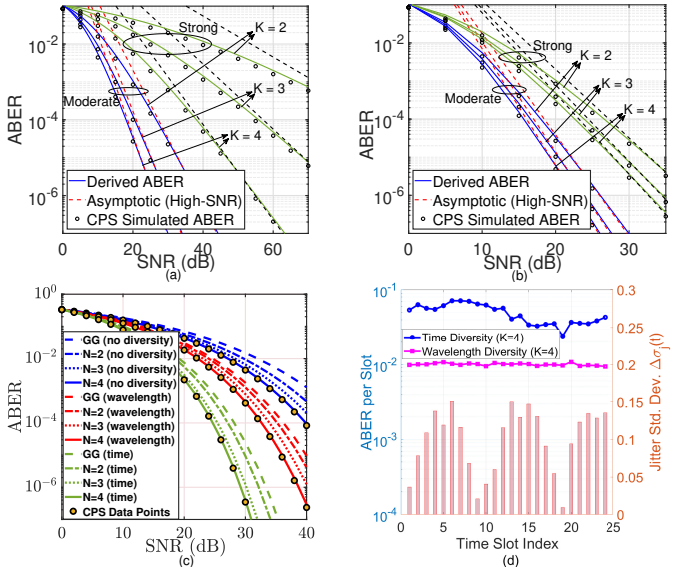

Fig. 2: Performance of the proposed N^*GG VFSO model: ABER vs. SNR for (a) wavelength diversity and (b) time diversity under moderate/strong turbulence; (c) comparison of layered N^*GG ($N > 1$) with conventional horizontal-equivalent GG ($N = 1$); (d) impacts of time-varying angular jitter.

Figs. 2 (a) and (b) show ABER performance under different turbulence. Close match of the exact analytical plots, CPS simulations, and high-SNR asymptotics across the SNR range confirms the correctness of the derived expressions. The high-SNR slopes match with the diversity orders in Table I. Fig. 2(c) benchmarks the proposed layered N^*GG model against the conventional GG model ($N = 1$). The CPS points confirm that larger N improves fidelity, with $N = 4$ offering up to $\approx 2.1\,\text{dB}$ SNR gain at ABER $= 10^{-4}$ under strong turbulence. Notably, the gain saturates beyond $N = 4$, implying that for typical stratosphere-to-ground paths, 4 layers capture most altitude-dependent turbulence variation. This finding provides a practical guideline for selecting optimum N without undue computational overhead. Close agreement between the derived ABER results and CPS-based Monte-Carlo simulations is because the Meijer-G representations employed for the Q-function and exponential terms are mathematically tight over the full SNR range. Moreover, the multiplicative N^*GG fading structure preserves the dominant statistical tails that govern error probability, ensuring a close match between analytical and simulation results. Fig. 2(d) shows the impact of angular jitter on per-slot ABER with $K = 4$ alongside the jitter variance $\Delta\sigma_j(t)$. Time diversity shows abrupt ABER spikes when jitter increases, whereas wavelength diversity remains more robust. Thus, wavelength diversity performs better under time-varying jitter, while time diversity offers gain at low jitter.

Fig. 3(a) captures ABER sensitivity to turbulence parameters (α, β). Intuitively, larger (α, β) (weaker turbulence) improves the performance of all schemes, but time diversity consistently offers low ABER across the parameter space. Interestingly, the relative advantage of time diversity increases for asymmetric turbulence (e.g., high α and low β), where scintillation becomes dominated by a single scale. This robustness under skewed turbulence statistics is valuable for real deployments with imbalanced atmospheric conditions. Fig. 3(b) shows the impact of pointing-error variance σ_s/a, normalized beamwidth w_z/a, and rotation parameter ρ/a under moderate turbulence. Increasing σ_s/a degrades the performance in all schemes, but wavelength diversity maintains a shallower ABER slope due to its partially uncorrelated

[1]While our analysis is primarily theoretical, the numerical parameters are within practical operating ranges. For example, gimbal-stabilized optical terminals on airborne platforms can provide pointing accuracies below 0.5 mrad [1], [13], which matches our jitter model. Also, wavelength diversity is supported by standard optical modules, and slot-level timing decorrelation is achievable with clock precisions in modern digital hardware. Thus, the noted diversity gains are not idealized but consistent with achievable system-level constraints. Further, the reported gains indicate maximum diversity leverage; practical implementations may observe smaller gains due to tracking latency, power imbalance, or wavelength-specific detector inefficiencies.

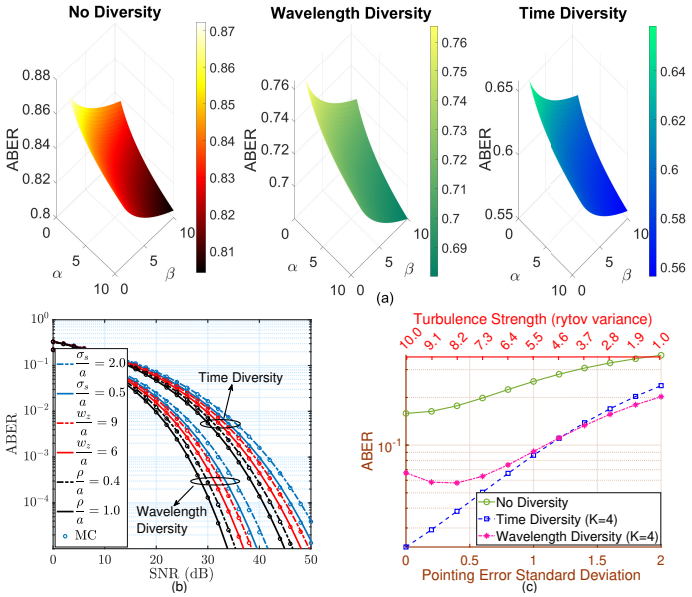

Fig. 3: Robustness analysis of transmit diversity schemes: (a) ABER sensitivity to turbulence parameters (α, β); (b) effect of pointing-error variance σ_s/a, normalized beamwidth w_z/a, and rotation parameter ρ/a on ABER; (c) performance under combined turbulence fading and pointing errors.

pointing losses across wavelengths. This effect is amplified when ρ/a is near unity, indicating optimal receiver alignment in at least one wavelength branch. Computationally, increasing N from 2 to 4 in our implementation raised runtime by $\approx 65\%$ but reduced analytical SNR error compared to the simulated performance by $\approx 1.2\,\text{dB}$ at ABER $= 10^{-4}$, suggesting $N = 3$ or 4 as optimal for balancing fidelity and complexity. These trends, combined with the validated asymptotics under varying (α, β), confirm that the proposed layered model not only outperforms the horizontal-equivalent GG benchmark but also provides clear operational guidelines in HAP-to-ground FSO deployments. Fig. 3(c) shows the combined impact of pointing error and turbulence. Time diversity outperforms wavelength diversity under strong turbulence and small pointing error. However, at weak turbulence and higher pointing error, wavelength diversity is more effective. In wavelength diversity, the initial drop in ABER occurs as turbulence decreases, showing wavelength diversity effectively mitigates very minimal pointing errors. At a higher pointing error, ABER increases despite decreasing turbulence strength, indicating the increased impact of misalignment. A summary of these operating regions along with the expected gains is given in Table II as a design reference in VFSO links [2].

V. Conclusion

This letter investigated error performance of concatenated HAP-to-ground VFSO link under two transmit diversity schemes. The accuracy of the analysis was verified by Monte-Carlo simulations of VFSO channel using CPS method. The numerical studies showed that, time diversity offers better error performance compared to wavelength diversity when optical turbulence dominates, whereas wavelength diversity performs better when the VFSO link undergoes severe pointing error.

[2]In dense multi-HAP deployments, co-channel interference (CCI) may arise when several VFSO links use the same optical resources. The layered model adopted here naturally extends to interference-limited scenarios, as each interfering path would experience altitude-dependent turbulence and pointing error statistics. The advantage of time versus wavelength diversity depends on whether interference varies more strongly across time slots or across optical bands. A detailed CCI-aware extension is left for future work, but this observation highlights that the layered channel model remains applicable and provides a tractable basis for analyzing interference-limited VFSO networks.

TABLE II: Design guide: Time diversity versus wavelength diversity

Case/Sensitivity	**Best**	**Key insight/Gain (ABER limit 10^{-4})**
Strong turbulence, low pointing error	Time diversity	Temporal decorrelation across K slots; **+7.5 dB**; slot spacing $>$ coherence time
High pointing error, low turbulence	Wavelength diversity	Decorrelation across K wavelengths; **+10 dB**; pick $\Delta\lambda$ to lower correlation
Layer granularity (N)	Both	N = 3-4 gives good model fidelity; complexity ↑ with N; practical $N \leq 4$
(α, β) sensitivity	Time diversity	Smaller $(\alpha, \beta) \Rightarrow$ stronger turbulence; ADO grows with time diversity
Mixed regime	Switch/ hybrid	$\sigma_j \leq 0.3$ mrad, $\sigma_R^2 \geq 7 \Rightarrow$ Time; $\sigma_j \geq 0.8$ mrad, $\sigma_R^2 \leq 4 \Rightarrow$ Wavelength

References

[1] M. S. Bashir and M.-S. Alouini, "Free-space optical MISO communications with an array of detectors," *IEEE Open J. Commun. Soc.*, vol. 1, pp. 1765-1780, Nov. 2020.

[2] S. Li et al., "Performance evaluation of the vertical layered UWOC system with spatial diversity," *IEEE Wirel. Commun. Lett.*, vol. 13, no. 7, pp. 1873-1877, Jul. 2024.

[3] H. E. Nistazakis and G. S. Tombras, "On the use of wavelength and time diversity in optical wireless communication systems over Gamma–Gamma turbulence channels," *Opt. & Laser Technol.*, vol. 44, no. 7, pp. 2088–2094, Oct. 2012.

[4] J. Ji et al., "Design and investigation of 10 Gb/s FSO wiretap channel using OCDMA time-diversity reception," *IEEE Photon. J.*, vol. 12, no. 3, pp. 1-12, June 2020.

[5] S.-J. Kim & S.-K. Han, "Power efficiency analysis of spatial diversity based vertical FSO links with pointing error in multiple beam transmissions," *IEEE Access*, vol. 10, pp. 129925-129931, Dec. 2022.

[6] N. Tiwari et al., "Concatenated vertical channel modeling and performance analysis for HAP-based optical networks," *IEEE Photon. J.*, vol. 16, no. 5, pp. 1–14, Oct. 2024.

[7] L. C. Andrews and R. L. Phillips, "Laser beam propagation through random media," *Second Edition*, Sep 2005.

[8] N. Tiwari et al.,"Modeling of channel asymmetry in HAP-based optical wireless communication," in *Proc. NCC*, India, 2023.

[9] M. Singh et al., "Performance analysis in spectral-amplitude-coding-optical-code-division-multiple-access using identity column shift matrix code in free space optical transmission systems," *Opt Quant Electron*, vol. 56, no. 795, Mar 2024.

[10] E.E. Elsayed, "Investigations on modified OOK and adaptive threshold for wavelength division multiplexing free-space optical systems impaired by interchannel crosstalk, atmospheric turbulence, and ASE noise," *J Opt*, Jun 2024.

[11] G. Xu et al., "Outage Probability and Average BER of UAV-Assisted Dual-Hop FSO Communication With Amplify-and-Forward Relaying," in *IEEE Trans. Veh. Tech.*, vol. 72, no. 7, pp. 8287-8302, Jul 2023.

[12] G. Xu et al., "Outage Probability and Average BER of UAV-Assisted RF/FSO System for Space–Air–Ground Integrated Networks Under Angle-of-Arrival Fluctuations," *IEEE Internet Things J.*, vol. 11, no. 20, pp. 34009-34023, Oct.2024.

[13] X. Tang et al., "Experimental demonstration of polarisation shift keying in the free space optical turbulence channel," in *Proc. IEEE ICC Wrkshps, China*, pp. 31–36, Aug. 2012.

[14] *Wolfram Research.* Accessed: Mar 2025, [online.] Available: https://functions.wolfram.com.

[15] M. Chiani et al., "New exponential bounds & approximations for the computation of error probability in fading channels," *IEEE Trans. Wirel. Commun.*, vol. 2, no. 4, pp. 840–845, Jul. 2003.

[16] K. Prabu et al., "Analysis of PolSK based FSO system using wavelength and time diversity over strong atmospheric turbulence with pointing errors", *Opt. Commun.*, vol. 324, pp. 318–323, Aug. 2014.